Enhanced ^{13}C NMR detects extended reaction networks in living cells

Jensen, Pernille Rose; Sannelli, Francesca; Stauning, Ludvig Tving; Meier, Sebastian

Published in:
Chemical Communications

Link to article, DOI:
10.1039/d1cc03838a

Publication date:
2021

Document Version
Peer reviewed version

COMMUNICATION

Enhanced ^{13}C NMR Detects Extended Reaction Networks in Living Cells

Pernille Rose Jensen[1]*, Francesca Sannelli[2$], Ludvig Tving Stauning[1,2$], and Sebastian Meier[2]*

Received 00th January 20xx,
Accepted 00th January 20xx

DOI: 10.1039/x0xx00000x

Insights into intracellular chemistry have remained sparse, but would be impactful for the advancement of biomedicine and bioproduction. A suitable ^{13}C NMR approach provides improvements in sensitivity that make extended reaction networks and assay time windows, previously inaccessible cell densities and relative flux measurements accessible in living cells.

All living entities coordinate their energy and material demand through metabolism. These tasks are intertwined with the need to balance redox chemistry and combat oxidative damage.[1] The most central metabolic pathways bear promise for therapeutic targets and future sustainable production. The mechanistic details even of the most central pathways remain incompletely understood.[1-3] Mechanistic understanding of intracellular reaction kinetics and product control hinges on suitable analytical capabilities. Such analytical capabilities would therefore promise to be impactful for the advancement of biomedicine and bioproduction.

Insight into intracellular reaction chemistry under natural conditions hinges on the use of minimally invasive methodology employing natural or near-natural substrates. NMR spectroscopy has been employed to study cellular reactions since more than four decades,[4] as NMR spectroscopy provides a high spectral resolution and detects nuclear isotopes rather than bulky non-natural groups. However, NMR spectroscopy suffers from the presence of background signals and from rather low signal amplitudes relative to the noise from the detection electronics. These problems can be somewhat mitigated by the use of cryogenically cooled detection electronics[5] and of isotope-enriched reactants for ^{13}C NMR. Nevertheless, in-cell NMR studies require high cell densities and acquisition times that prohibit the detection of pre-steady state kinetics.[6] In addition to the minimally invasive isotope labelling,[7] a physical labelling approach termed hyperpolarization has gained some popularity.[8] Hyperpolarization temporarily enhances nuclear spin alignment by four orders of magnitude. This non-equilibrium state fades however with a rate ($1/T_1$) that is characteristic for the site of the nucleus. In addition, spin alignment is consumed by each experimental observation, thus limiting the timescale and number of observations during which sensitive observations are possible. Thus, hyperpolarized NMR spectroscopy has mainly been used to observe one or few reaction steps[9-11] or fast glycolytic reactions for kinetic analysis in model organisms and mammals.[12-15] Common approaches to studying metabolism use extracellular detection with NMR spectroscopy[16-18] or mass spectrometry for concentration measurements,[19,20] after samples have been stabilized by the quenching of cellular activities.[21,22] Circumventing the limited sensitivity of in-cell NMR spectroscopy, the need for high cell densities and the need for quenching of cellular activities will permit addressing additional biological information (Scheme 1).

The current study explores the information gain in cellular assays when using optimized signal detection schemes. An in-cell assay at discrete time points is proposed, where each time point corresponds to a sensitivity-optimized single ^{13}C NMR

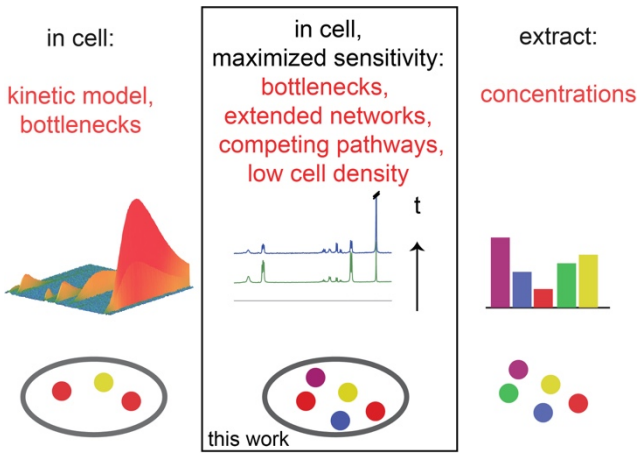

Scheme 1. Schematic overview of NMR strategies observing real-time reactions in cells with low sensitivity (left; metabolites depicted as circles) or analyzing stabilized extracts (right, bars indicating measurements of stabilized concentrations). In-cell data with maximized sensitivity provides complimentary information by bridging the time scales and sensitivities that are accessible with in-cell and out-of-cell measurements.

[a] *Department of Health Technology Technical University of Denmark Elektrovej 349 2800-Kgs. Lyngby, Denmark; E-mail: peroje@dtu.dk*
[b] *Department of Chemistry Technical University of Denmark Kemitorvet, Bygning 207, 2800 Kgs. Lyngby, Denmark; E-mail: semei@kemi.dtu.dk*
[$] *These authors contributed equally to this work*
† Footnotes relating to the title and/or authors should appear here.
Electronic Supplementary Information (ESI) available: [details of any supplementary information available should be included here]. See DOI: 10.1039/x0xx00000x

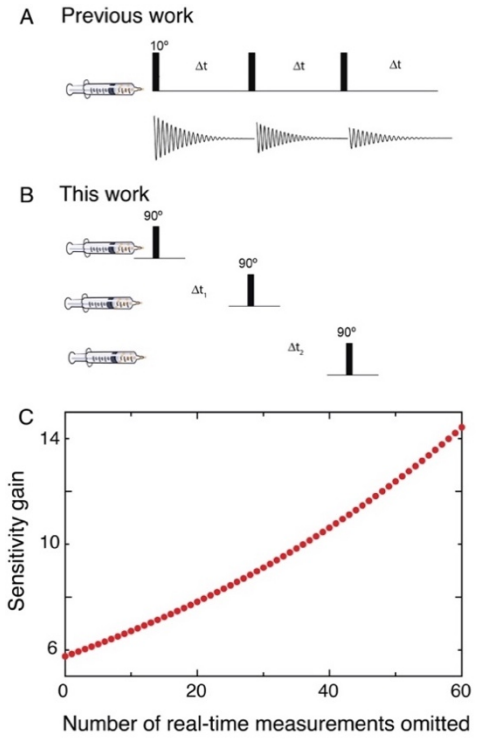

Fig. 1. (A) Conventional approach to acquiring time-resolved hyperpolarized NMR measurements. Non-equilibrium hyperpolarization is consumed by each experimental observation and small flip angles are needed to maintain signal for repeated measurements. (B) Repetition of experiments with maximum sensitivity readout. (C) Sensitivity gains for the discontinuous approach displayed in (B) relative to real-time measurements with 10° detection pulses (A), as a function of omitted real-time measurements.

experiment (Fig. 1). Compared to conventional data acquisition schemes, this approach enhances the signal-to-noise ratio by orders of magnitude. Measurements of slower processes on longer time scales will then become feasible for pathways that producs small compounds with slow relaxation. Beyond extended observation time spans for hyperpolarized NMR, this approach importantly also will bring measurements at low cell densities into the realm of possibility, and enable the observation of extended reaction networks rather than short reaction sequences only.

Hyperpolarized glucose was produced with the dissolution DNP (D-DNP) methodology using [U-^{13}C,^{2}H] and [1-^{13}C,^{2}H] isotopologues with T_1 of approximately 15 and 13 s, respectively. The D-DNP methodology polarizes ^{13}C nuclear spins of glucose to 40% of full nuclear spin alignment in the solid state. Further improvement of the spin polarization was outside the scope of the current study. Instead, the use of time-discrete measurements detecting all hyperpolarization for optimal sensitivity was pursued herein. This approach complements conventional kinetic measurements that use small flip angle (θ) pulses for time-resolved measurements (Fig. 1A,B).[23,24] The conventional approach slowly consumes hyperpolarization and detects only a fraction F of the maximum signal that is given as $F = \sin\theta \times \cos^{n}\theta$ following n previous measurements (time points). Scheme 1C exemplifies the expected improvements in signal-to-noise ratio for time-discrete measurements relative to time-resolved measurements with 10° pulses for the same intracellular process. Equivalent curves are shown in Fig. S1 for various flip angle pulses.

Theoretical improvements were compared to measurements using yeast as a model organism for method development. All spectra were acquired in an 11.7 T magnet equipped with a cryogenically cooled detection electronics. A kinetic measurement using approximately 10° flip angle pulses is shown in Fig. 2. An 1D ^{13}C NMR spectrum was acquired every 0.5 seconds after injection of 7 mM hyperpolarized [U-^{13}C,^{2}H] glucose. Time-discrete measurements using a selective 90° pulse for readout of the carbonyl region were acquired for comparison after 10, 20 and 50 seconds. Experimentally achieved gains in sensitivity at these times by time discrete 1D ^{13}C NMR spectra were 9, 14 and 43-fold, when comparing signal-to-noise ratios of bicarbonate in discontinuous measurements to the measurement of Fig. 3. These increases are expected for a pulse angle in the kinetic experiment of approximately 12° after omitting 20, 40 and 100 measurements, respectively. Signal-to-noise ratios increase with the square root of repetitions due to the accumulation of non-coherent noise. Hence, enhancements of one to two orders of magnitude through the described change of detection scheme would be difficult to achieve when summing up repeated measurements. Fig. 3 compares the ^{13}C NMR spectra obtained after 10 and 20 seconds with the sum of all time points from 12 kinetic measurements acquired under identical conditions to support this notion. The optimal timing for the 90° pulse depends on the T_1 of the product, while the dependence of the rate constant is negligible in regimes reasonable for in cell experiments, as shown in simulations that are displayed in Fig. S2.

The described gain in sensitivity opens various novel avenues for functional assays in living cells: (i) Signal enhancements are particularly striking for the later time points of an intracellular reaction and the time scale of hyperpolarized NMR (up to the low minute time scale) and of non-hyperpolarized NMR (low minutes time scale and above) can be bridged; (ii) more expanded parts of the intracellular reaction network should become observable; (iii) lower cell densities should become tractable under biologically more relevant settings, and (iv) accurate quantifications of network responses should become viable. Thus, a sensitive detection scheme could

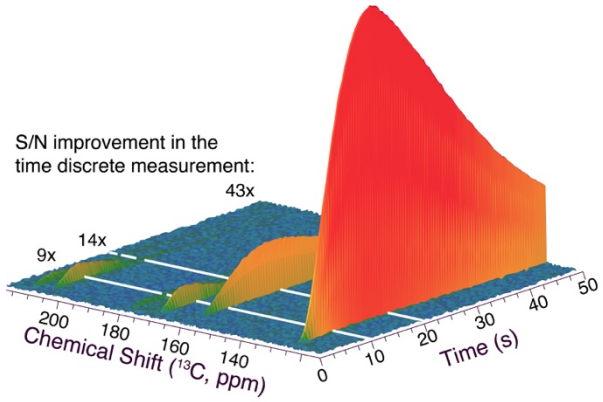

Fig. 2. Real-time kinetic experiment and experimental gains in sensitivity, if acquiring discrete spectra after 10, 20 or 50 seconds.

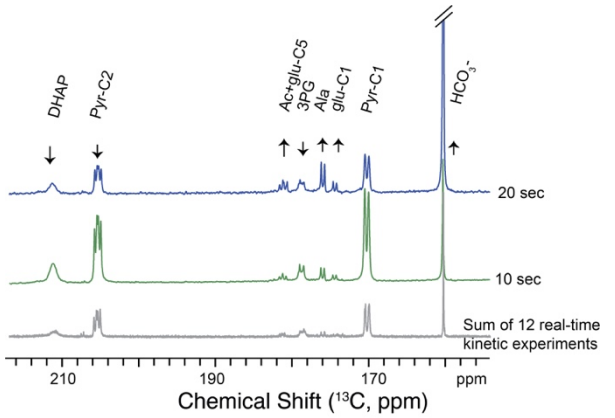

Fig. 3. 1D ^{13}C NMR spectra after 10 and 20 seconds, compared to the sum spectra of 100 time points each from twelve repeated kinetic experiments akin to the one displayed in Fig. 2.

provide complementary information to real-time measurements with lower sensitivity, but higher temporal resolution. Such measurements focussing on high temporal resolution had identified major bottlenecks and had shown mechanistic changes in the start-up of glycolysis.[6,19] With the proposed approach, kinetic bottlenecks and relative changes in intracellular activity may be identified by relative changes in signal ratios, without a kinetic model based on real-time data. Such an approach can complement common attempts to track metabolites in a time-resolved manner. The discontinuous assay hinges on reproducible measurements, and a satisfactory relative standard deviation below 8% for signal areas in quadruplicate was determined (Fig S3).

The measurements of Fig. 3 show that new network products become observable with the applied approach. Sensitivity gains with the proposed sampling schemes translate to sufficient signal-to-noise, if products with long T_1 times are formed. Comparison to authentic standard spectra and data bases show that the newly observed signals do not derive from glycolytic intermediates. Rather, authentic standard spectra indicate that signals at 174.5 ppm and 181.3 ppm (relative to pyruvate at 26.6, 170.3 and 205.1 ppm) can be tentatively assigned to glutamate (Fig. S4). Rapid injection 2D ^{1}H-^{13}C spectroscopy validates that citric acid cycle intermediates are labelled on the low minute timescale (Fig. S5). Notably, each measurement of in cell 1D ^{13}C NMR spectra requires 0.3 seconds, opposite to the ^{1}H-^{13}C spectra of 2 minutes duration. The sidechain carboxylic acid signal at 181.3 ppm partly overlaps with another non-glycolytic signal that is consistent with the formation of acetate. Difference spectra between labelling of cellular metabolites after 10 seconds and after 20 seconds distinguish between end products from a more extended reaction network (Fig. 4, positive signals) and glycolytic intermediates (Fig. 4, negative signals due to decreasing labelling after 10 seconds).

Notably, all glycolytic intermediates and other metabolites beyond carbon dioxide and bicarbonate would be on the brink of being non-detectable with real-time measurements of 14-fold lower sensitivity (Fig. 2) after 20 seconds. With the suggested acquisition scheme, these metabolites remain

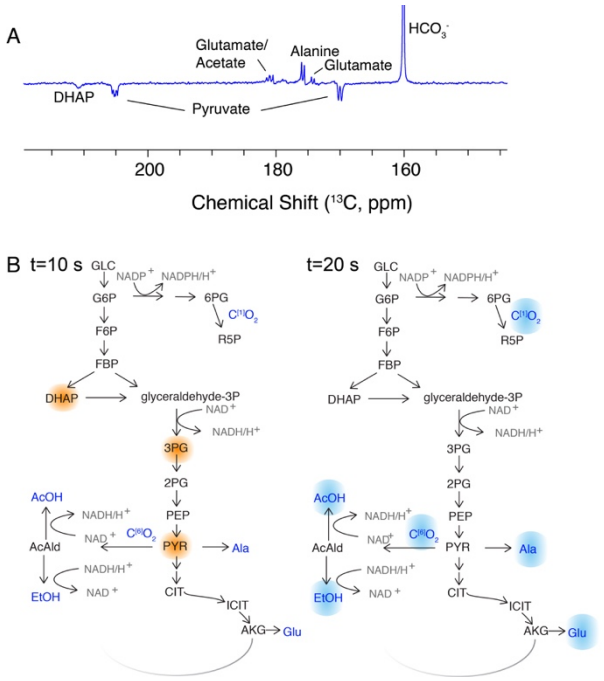

Fig. 4. (A) The difference spectrum between spectra acquired after 20 and after 10 seconds highlights the decay of glycolytic intermediates and the allows the direct identification of products from diverse pathways. (B) Schematic overview of chemicals that are more strongly labelled 10 seconds after a glucose pulse (orange) or 20 seconds after a glucose pulse (blue).

detectable also beyond one minute after injection of tracer (Fig. S6). The main compounds that are labelled with hyperpolarized magnetization after one minute include pyruvate, alanine and glutamate. This observation is consistent with previously determined metabolite pools indicating that pyruvate is the most abundant glycolytic metabolite (at 10^{-2} M), while alanine and glutamate, which are accessible from pyruvate, are the most abundant amino acids (2.2×10^{-2} M and 3.9×10^{-2} M, respectively).[2] Hence, observed distributions of glucose signal one minute after injection was consistent with a redistribution towards the steady state pool of intracellular chemicals.

Importantly, the increased sensitivity of the current sampling scheme also directly translates to the use of low cell densities. S/N ratios above 30 for metabolites after 20 seconds of glucose influx at OD ~30 in the NMR sample tube indicate that meaningful cellular assays can be conducted at 10-fold lower cell densities (Fig. S7). Higher S/N ratios for label influx at times of less than 20 seconds imply that even lower cell densities can be useful for monitoring rapid product formation in the living cells (Fig. S7B shows a ^{13}C NMR spectrum after 10 seconds for OD=1).

Finally, we assessed relative signal influx into different catalytic pathways, one of which had been considered inaccessible to D-DNP NMR.[15] The carbon dioxide and bicarbonate signals that are formed from [U-^{13}C,^{2}H] glucose can derive either from glycolysis and alcoholic fermentation, or from the pentose phosphate pathway. In order to distinguish between the use of the two pathways, hyperpolarized [1-^{13}C,^{2}H] glucose substrate was used (Fig. 5).[25] The ^{13}C label ends in the C2 position of ethanol in alcoholic fermentation, but in

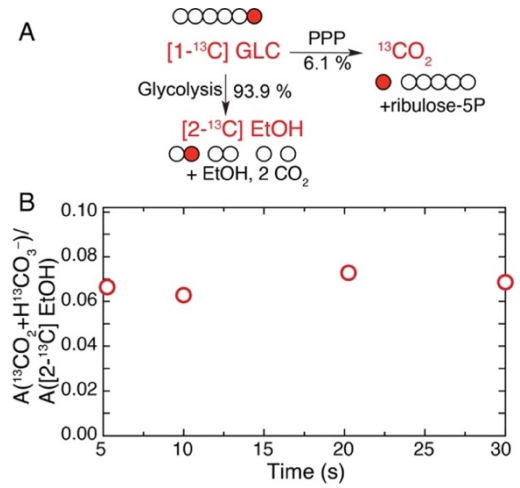

Fig. 5. (A) Schematic overview of the fate of the label in [1-^{13}C,^{2}H] glucose in glycolysis and the pentose phosphate pathway in yeast. (B) Ratiometric measurement of hyperpolarized [1-^{13}C,^{2}H] glucose influx into glycolysis and pentose phosphate pathway.

CO_2/HCO_3^- in the pentose phosphate pathway, which has been considered non-accessible in D-DNP assays in yeast.[15] However, we find that hyperpolarized [1-^{13}C,^{2}H] glucose can be found to enter the pentose phosphate pathway and glycolysis at ratios 6.1%/93.9%, consistent with estimates from literature (3%[26]-10%[27] relative pentose phosphate pathway flux in *S. cerevisiae*, Fig. S8). Hence, accurate flux distributions can be obtained for pathways that were deemed unobservable with time-resolved D-DNP NMR measurements. These observations confirm that new information can be assessed by sensitivity optimized discontinuous assays.

In conclusion, a time-discrete in-cell D-DNP NMR approach is presented using intracellular reactions in yeast as a case study. A suitable analytical approach provides orders of magnitude improvements in sensitivity of single scan ^{13}C NMR relative to real-time kinetic measurements. This improvement makes more extensive reaction networks, longer assay time windows, previously inaccessible cell densities, and relative fluxes into competing reaction pathways accessible. Albeit often considered exceedingly difficult, studies of the operational mode of intracellular chemistry can thus be significantly expanded with available NMR instrumentation and suitably adapted measurement schemes.

The authors gratefully acknowledge support by the Danish National Research Foundation (DNRF124) and by the Independent Research Fund Denmark (Green transition programme, grant 0217-00277A). 800 MHz NMR spectra NMR spectra were recorded at the NMR Center DTU, supported by the Villum Foundation. D-DNP NMR data were acquired with equipment partially funded by the Novo Nordisk Foundation (NNF19OC0055825).

Conflicts of interest

There are no conflicts to declare.

Notes and references

1 A. Stincone, A. Prigione, T. Cramer, M. M. C. Wamelink, K. Campbell, E. Cheung, V. Olin-Sandoval, N.-M. Grüning, A. Krüger, M. Tauqeer Alam, M. A. Keller, M. Breitenbach, K. M. Brindle, J. D. Rabinowitz and M. Ralser, *Biol.l Rev.*, 2015, **90**, 927-963.
2 J. O. Park, L. B. Tanner, M. H. Wei, D. B. Khana, T. B. Jacobson, Z. Zhang, S. A. Rubin, S. H.-J. Li, M. B. Higgins, D. M. Stevenson, D. Amador-Noguez and J. D. Rabinowitz, *Nat. Chem. Biol.*, 2019, **15**, 1001-1008.
3 Michelle F. Clasquin, E. Melamud, A. Singer, Jessica R. Gooding, X. Xu, A. Dong, H. Cui, Shawn R. Campagna, A. Savchenko, Alexander F. Yakunin, Joshua D. Rabinowitz and Amy A. Caudy, *Cell*, 2011, **145**, 969-980.
4 R. G. Shulman, T. R. Brown, K. Ugurbil, S. Ogawa, S. M. Cohen and J. A. den Hollander, *Science*, 1979, **205**, 160.
5 H. Kovacs, D. Moskau and M. Spraul, *Prog. Nucl. Magn. Res. Spectrosc.*, 2005, **46**, 131-155.
6 P. R. Jensen, M. R. A. Matos, N. Sonnenschein and S. Meier, *Anal. Chem.* 2019, **91**, 5395-5402.
7 C. Jang, L. Chen and J. D. Rabinowitz, *Cell*, 2018, **173**, 822-837.
8 J. H. Ardenkjaer-Larsen, B. Fridlund, A. Gram, G. Hansson, L. Hansson, M. H. Lerche, R. Servin, M. Thaning and K. Golman, *Proc. Natl. Acad. Sci. U.S.A.*, 2003, **100**, 10158-10163.
9 M. E. Merritt, C. Harrison, C. Storey, F. M. Jeffrey, A. D. Sherry and C. R. Malloy, *Proc. Natl. Acad. Sci. U.S.A.*, 2007, **104**, 19773.
10 M. A. Schroeder, L. E. Cochlin, L. C. Heather, K. Clarke, G. K. Radda and D. J. Tyler, *Proc. Natl. Acad. Sci. U.S.A.*, 2008, **105**, 12051.
11 A. Comment and M. E. Merritt, *Biochemistry*, 2014, **53**, 7333-7357.
12 S. Meier, P. R. Jensen and J. O. Duus, *FEBS Lett.*, 2011, **585**, 3133-3138.
13 S. Meier, M. Karlsson, P. R. Jensen, M. H. Lerche and J. O. Duus, *Mol. BioSys.*, 2011, **7**, 2834-2836.
14 T. Harris, H. Degani and L. Frydman, *NMR Biomed.*, 2013, **26**, 1831-1843.
15 K. N. Timm, J. Hartl, M. A. Keller, D.-E. Hu, M. I. Kettunen, T. B. Rodrigues, M. Ralser and K. M. Brindle, *Magn. Reson. Med.*, 2015, **74**, 1543-1547.
16 I.A. Lewis, S.C. Schommer, B. Hodis, K.A. Robb, M. Tonelli, W.M. Westler, M.R. Sussman and J.L. Markley, *Anal. Chem.*, 2007, **79**, 9385-9390.
17 M. H. Lerche, D. Yigit, A. B. Frahm, J. H. Ardenkjær-Larsen, R. M. Malinowski and P. R. Jensen, *Anal. Chem.*, 2018, **90**, 674-678.
18 A.M. Weljie, J. Newton, P. Mercier, E. Carlson and C.M. Slupsky, *Anal. Chem.*, 2006, **78**, 4430-4442.
19 B. D. Bennett, J. Yuan, E. H. Kimball and J. D. Rabinowitz, *Nat. Protoc.*, 2008, **3**, 1299-1311.
20 B. D. Bennett, E. H. Kimball, M. Gao, R. Osterhout, S. J. Van Dien and J. D. Rabinowitz, *Nat. Chem. Biol.* 2009, **5**, 593-599.
21 A. B. Canelas, C. Ras, A. ten Pierick, J. C. van Dam, J. J. Heijnen and W. M. van Gulik, *Metabolomics*, 2008, **4**, 226-239.
22 S. Dietmair, N. E. Timmins, P. P. Gray, L. K. Nielsen and J. O. Krömer, *Anal. Biochem.*, 2010, **404**, 155-164.
23 K. Golman, R. i. Zandt, M. Lerche, R. Pehrson and J. H. Ardenkjaer-Larsen, *Cancer Res.*, 2006, **66**, 10855.
24 S. Bowen and C. Hilty, *Angew. Chem.*, 2008, **47**, 5235-5237.
25 P. R. Jensen and S. Meier, *Analyst*, 2016, **141**, 823-826.
26 J. O. Park, S. A. Rubin, Y.-F. Xu, D. Amador-Noguez, J. Fan, T. Shlomi and J. D. Rabinowitz, *Nat. Chem. Biol.*, 2016, **12**, 482-489.
27 L. M. Blank, F. Lehmbeck and U. Sauer, *FEMS Yeast Res.*, 2005, **5**, 545-558.
28

